VOL. 17, NO. 5 AIAA JOURNAL MAY 1979

ARTICLE NO. 77-1370

Spectra of Turbulent Static Pressure Fluctuations in Jet Mixing Layers

B. G. Jones,* R. J. Adrian,† C. K. Nithianandan‡
University of Illinois at Urbana-Champaign, Ill.
and
H. P. Planchon Jr.§
Westinghouse Electric Corporation, Madison, Pa.

Spectral similarity laws are derived for the power spectra of turbulent static pressure fluctuations by application of dimensional analysis in the limit of large turbulent Reynolds number. The theory predicts that pressure spectra are generated by three distinct types of interaction in the velocity fields: a fourth-order interaction between fluctuating velocities, an interaction between the first-order mean shear and the third-order velocity fluctuations, and an interaction between the second-order mean shear rate and the second-order fluctuating velocity. In the inertial subrange the spectra associated with these three interaction modes exhibit $k^{-7/3}$, $k^{-9/3}$, and $k^{-11/3}$ power laws, respectively. Measurements of one-dimensional power spectra of the turbulent static pressure fluctuations in the driven mixing layer of a subsonic, circular jet are presented, and the spectra are examined for evidence of spectral similarity. Spectral similarity is found for the low wavenumber range when the large-scale flow on the centerline of the mixing layer is self-preserving. The data are also consistent with the existence of universal inertial subranges for the spectra of each interaction mode.

I. Introduction

THE structure of the fluctuating static pressure field is an important characteristic of turbulent flow whose understanding is relevant not only to the basic theory of turbulence dynamics, but also to several immediately applicable areas of turbulence research such as the development of higher-order, semiempirical models of turbulence, in which the pressure-velocity covariance is of prime importance (Refs. 1, 2, and many others), and the prediction of noise generated by turbulent flow using a dilatational model[3,4] in which the space-time correlation of the fluctuating static pressure is the primary empirical input. Other exemplary applications are flow-induced vibrations of structures and wave propagation through turbulent media.

The spectrum of the pressure fluctuations provides the simplest statistical description of the spatial structure of the turbulent pressure field, and it is likely that this spectral structure will be as important in understanding the dynamics of the pressure field as the turbulent velocity spectrum has been in describing the basic dynamics of turbulent velocity fields. Using a dimensional analysis similar to the customary analysis of turbulent velocity spectra,[5,6] George[7] concluded that the pressure spectrum would possess an equilibrium range that scaled with Kolmogorov variables and an inertial subrange in which the spectrum obeyed a $k^{-7/3}$ power law. This power law was consistent with Batchelor's[5] prediction for isotropic turbulence.

Turbulence pressure spectra have been measured by Fuchs,[8] Planchon,[4] Hammersley,[9] and Beuther et al.[10,11]; Fuchs[8] used a shrouded microphone, Planchon[4] and Hammersley[9] used a bleed-type unsteady pressure tranducer of the kind described by Spencer and Jones,[12] and Beuther et al.[10,11] used a standard 0.305-cm-diam pitot static tube coupled to a small condenser microphone as described in Arndt and Nilsen.[13] Planchon's[4] data were taken on the centerline of the driven mixing layer surrounding the potential core of a 6.35-cm-diam, 91.4 ms^{-1} free circular jet and are directly comparable to the Beuther et al.[10,11] data which were taken on the mixing layer centerline of a 3.05-cm-diam, 30.5 ms^{-1} circular jet. The latter data in preliminary form were presented by George[5] and appeared to verify his findings. Likewise, when plotted using Kolmogorov scaling, Planchon's[4] data also appeared to support the $k^{-7/3}$ power law, although the data did exhibit small, consistent descrepancies with the $k^{-7/3}$ behavior.[14]

Recently, Beuther et al.[10,11] proposed a simple flow model consisting of isotropic turbulence plus a constant mean shear. This model predicts the turbulent-turbulent component of the pressure spectrum (and its $k^{-7/3}$ law) plus an additional pressure spectral component due to interactions of the fluctuating velocities with the mean shear field. This component, referred to as the shear pressure spectrum, exhibits a $k^{-11/3}$ power law in the inertial subrange. The same authors also note the possibility of a third component possessing a k^{-3} power law. In a companion paper, George and Beuther[15] showed that the fourth-order velocity spectrum obeys a $k^{-5/3}$ law so that stagnation velocity contamination of unsteady pressure probes will not produce a spectrum that is confounded with the true pressure spectra.

The purposes of this paper are first to present a simple, independent analysis of the pressure spectrum in flows with mean shear that is based on dimensional reasoning and is intended to develop the scaling laws for spectral similarity analysis of the data; and second, to present Planchon's[4] spectral data, which have been reanalyzed in terms of these new similarity results and presented with auxilliary velocity field data which are pertinent to their interpretation. These data provide an independent test of the similarity theory. In addition, since this flow is very similar to the flow studied by Beuther et al.,[10,11] the spectral data can be compared directly, and some inference can be drawn regarding the accuracy of the two different pressure transducers used in these studies. In

Presented as Paper 77-1370 at the AIAA 4th Aeroacoustics Conference, Atlanta, Ga., Oct. 3-5, 1977; submitted Oct. 6, 1977, revision received Sept. 1, 1978.

Index categories: Jets, Wakes, and Viscid-Inviscid Flow Interactions; Aeroacoustics; Subsonic Flow.

*Professor of Nuclear and of Mechanical Engineering. Member AIAA.

†Associate Professor of Theoretical and Applied Mechanics.

‡Research Assistant in Nuclear Engineering.

§Research Engineer.

view of the difficulties associated with the design of pressure transducers which are sensitive to static pressure fluctuations but insensitive to contamination by the velocity field, this purpose is, perhaps, as important as the examination of the similarity laws.

II. Theory

Pressure Intensity, Correlation and Spectrum

For an unbounded, incompressible turbulent flow the fluctuating static pressure at position x (x_i) is given by[16]

$$p(x,t) = \frac{-\rho}{4\pi}\int_y \mathrm{d}^3y \; \frac{1}{|x-y|}\,\frac{\partial^2}{\partial y_i \partial y_j}\left[(U_i+u_i)(U_j+u_j) - \overline{(U_i+u_i)(U_j+u_j)}\right] \tag{1}$$

where the mean velocity U_i and the fluctuating velocity u_i are evaluated at position $y(y_i)$. Using this formula, the two-point spatial covariance function at location x (which we suppress for compactness in the argument) with separation vector r, defined as

$$C_{pp}(r) = \overline{p(x,t)p(x+r,t)} \tag{2}$$

can be written in terms of the velocity as:

$$C_{pp}(r) = \frac{\rho^2}{16\pi^2}\int_y\int_{y'} \mathrm{d}^3y\mathrm{d}^3y' \; \frac{M}{|x-y|\,|x+r-y'|} \tag{3}$$

where

$$M = \overline{\left[\frac{\partial^2}{\partial y_i \partial y_j}(U_iu_j + U_ju_i + u_iu_j - \overline{u_iu_j})\,\frac{\partial^2}{\partial y'_k \partial y'_\ell}\right.}$$
$$\left.\overline{(U'_ku'_\ell + U'_\ell u'_k + u'_ku'_\ell - \overline{u'_ku'_\ell})}\right] \tag{4}$$

The quantity M represents a general fourth-order interaction between the mean and fluctuating velocities at y and y'. It can be decomposed into three distinct types of interactions,

$$M = {}^{04}M + {}^{13}M + {}^{22}M \tag{5}$$

by expanding the product in M and grouping terms according to the powers of the mean velocity (first superscript) and fluctuating velocity (second superscript). Thus,

$${}^{04}M = \frac{\partial^4}{\partial y_i \partial y_j \partial y'_k \partial y'_\ell}\left(\overline{u_iu_ju'_ku'_\ell} - \overline{u_iu_j}\;\overline{u'_ku'_\ell}\right) \tag{6}$$

is a pure fourth-order fluctuation interaction,

$${}^{13}M = 2\left(\frac{\partial U_i}{\partial y_j}\,\frac{\partial^3}{\partial y_i \partial y'_k \partial y'_\ell}\,\overline{u_ju'_ku'_\ell} + \frac{\partial U'_k}{\partial y'_\ell}\,\frac{\partial^3}{\partial y'_k \partial y_i \partial y_j}\,\overline{u'_\ell u_iu_j}\right) \tag{7}$$

is a third-order fluctuation interaction with the first-order mean shear field, and

$${}^{22}M = 4\frac{\partial U_i}{\partial y_j}\,\frac{\partial U'_k}{\partial y'_\ell}\,\overline{\frac{\partial u_j}{\partial y_i}\,\frac{\partial u'_\ell}{\partial y'_k}} \tag{8}$$

is a second-order fluctuation interaction with the second-order mean shear field. Each of these terms represents a distinct physical mechanism which will be referred to as an interaction mode.

Substituting Eqs. (6-8) into Eq. (3) shows that the covariance is a sum of the covariances from the interaction modes,

$$C_{pp}(r) = {}^{04}C_{pp}(r) + {}^{13}C_{pp}(r) + {}^{22}C_{pp}(r) \tag{9}$$

Since the mean square pressure is just

$$\sigma_p^2 = C_{pp}(0) \tag{10}$$

it likewise follows that the total mean square pressure is the sum of the mean square pressure fluctuations generated by each mode

$$\sigma_p^2 = {}^{04}\sigma_p^2 + {}^{13}\sigma_p^2 + {}^{22}\sigma_p^2 \tag{11}$$

where ${}^{04}\sigma_p^2 = {}^{04}C_{pp}(0)$, etc.

As can be seen by inspecting Eqs. (6-8) the ${}^{13}M$ and ${}^{22}M$ modes both vanish in isotropic turbulence, wherein the mean shear is necessarily zero. Hence, the mean square pressure in isotropic turbulence is due solely to the ${}^{04}M$ mode interactions. In contrast, all three modes are present in either inhomogeneous or homogeneous anisotropic turbulence but, in regard to spectra, if the high wave number range exhibits local isotropy, then the ${}^{13}M$ mode may be very weak. In any case, the correlations and spectra of anisoptropic turbulence can be expected to differ substantially with the rather artificial case of isotropic turbulence.

The three-dimensional wavenumber spectrum of the pressure is defined by

$$\phi_{pp}(k) = \frac{1}{8\pi^3}\int_{-\infty}^{\infty} C_{pp}(r)e^{-jk\cdot r}\mathrm{d}^3r \tag{12}$$

and the more readily measured one-dimensional spectrum is defined by

$$F_{pp}(k_1) = \frac{1}{2\pi}\int_{-\infty}^{\infty} C_{pp}(r_1,0,0)e^{-jk_1r_1}\mathrm{d}r_1 \tag{13}$$

In terms of this spectrum the mean square pressure is given by

$$\sigma_p^2 = \int_{-\infty}^{\infty} F_{pp}(k_1)\mathrm{d}k_1 \tag{14}$$

wherein the integral extends over positive and negative wavenumbers because the spectrum defined in Eq. (13) is two-sided. As in the case of velocity spectra, it is convenient to define yet a third spectrum, called the pressure energy spectrum function, whose argument is a single scalar wave number. This spectrum is obtained by integrating Φ_{pp} over a spherical shell of radius $|k| = k$ in wavenumber space,

$$\Pi(k) = \int_{|k|=k} \Phi_{pp}(k)\mathrm{d}A(k) \tag{15}$$

where $\mathrm{d}A(k)$ is an area element of the shell. The relationship between F_{pp} and Π is

$$F_{pp}(k_1) = \frac{1}{2}\int_{k_1}^{\infty}\frac{\Pi(k)}{k}\mathrm{d}k \tag{16}$$

for isotropic turbulence.[17]

Equations (9), (12), (13), and (15) combine to give Π and F_{pp} as sums of three spectra, representing the three modes of interaction discussed earlier. Thus,

$$\Pi = {}^{04}\Pi + {}^{13}\Pi + {}^{22}\Pi \tag{17}$$

and

$$F_{pp} = {}^{04}F_{pp} + {}^{13}F_{pp} + {}^{22}F_{pp} \tag{18}$$

The remainder of this section is devoted to an attempt to delineate the characteristics of these spectral modes by simple dimensional arguments.

Dimensional Analysis

The ensuing analysis of the pressure spectrum is closely analogous to conventional analyses of the velocity spectrum (see Refs. 5, 6, 16, and 17). Specifically, it is assumed first that the turbulence Reynolds number is so large that there is a large separation between the low wavenumbers of the energy containing motions and the high wavenumbers at which viscous dissipation occurs. Second, the large-scale flow is assumed to be characterized by the turbulent velocity scale,

$$u=\left(\frac{\sigma_u^2+\sigma_v^2+\sigma_w^2}{3}\right)^{1/2} \tag{19}$$

and a single length scale ℓ corresponding to an integral scale. An appropriate scale for the mean shear rate is

$$S=\left(\frac{\partial U_i}{\partial x_j}\frac{\partial U_j}{\partial x_j}\right)^{1/2} \tag{20}$$

Third, while the flow may be inhomogeneous such that u, ℓ, and S all vary with position, it is assumed that these variations occur slowly, so that changes over one length scale are small. This last assumption, referred to as local homogeneity, allows us to treat $\ell(x)$, $u(x)$, and $S(x)$ as approximate constants evaluated at their local values.

Since ${}^{04}\Pi$, ${}^{13}\Pi$, and ${}^{22}\Pi$ correspond to distinctly different physical mechanisms, each spectrum must be analyzed separately. Consider first the ${}^{22}M$ mode spectrum. At large Reynolds numbers there will exist a range of relatively low wavenumbers in which the flow behaves in an essentially inviscid manner. The appropriate length scale for this range is ℓ, and since most of the energy in the pressure spectrum is contained in this range the appropriate scale of pressure is simply ${}^{22}\sigma_p$. Then the dimensionless spectrum function and wavenumbers are ${}^{22}\Pi/{}^{22}\sigma_p^2\ell$ and $k\ell$ respectively, and dimensional analysis requires that

$${}^{22}\Pi/{}^{22}\sigma_p^2\ell={}^{22}G_p(k\ell) \tag{21}$$

The function ${}^{22}G_p$ must be determined experimentally or by a more refined theory. In general, ${}^{22}G_p$ is not a universal function for all flows because it represents the large-scale structure of the flow, and this structure certainly differs from one type of turbulent flow to another. However, within any class of flows having the same large-scale structure, ${}^{22}G_p$ will clearly be universal. In particular, ${}^{22}G_p$ should be universal within a given class of self-preserving flows[16] because the structure of a self-preserving flow is constant, aside from changes in the scales of length, velocity, and pressure. These flows include the self-preserving regions of turbulent jets, wakes, and shear layers.

A simple estimate relating the pressure scale ${}^{22}\sigma_p$ to the scales of the velocity field can be obtained by non-dimensionalizing the integral for ${}^{22}\sigma_p$. Letting a tilde denote a quantity made dimensionless by one of the scales ℓ, u, or S, we find from Eqs. (3), (8), (10), and (11) that

$${}^{22}\sigma_p={}^{22}B^2\rho^2u^2S^2\ell^2 \tag{22}$$

where

$${}^{22}B^2=\frac{1}{4\pi^2}\int_{\tilde{y}}\int_{\tilde{y}'}\mathrm{d}^3\tilde{y}\mathrm{d}^3\tilde{y}'\left(\frac{1}{S}\frac{\partial U_i}{\partial y_j}\right)\times\left(\frac{1}{S}\frac{\partial U_k'}{\partial y_\ell'}\right)\frac{\partial^2}{\partial\tilde{y}_i\partial\tilde{y}_k'}\overline{\tilde{u}_j\tilde{u}_\ell'} \tag{23}$$

The dimensionless coefficient, ${}^{22}B^2$, is determined by the details of the large-scale structure of the velocity field, and it will depend on the Reynolds number and on characteristic structural parameters such as the ratios of the integral length scales in the x, y, and z directions and anisotropy ratios σ_u/u, σ_v/u, and σ_w/u. Equation (22) is consistent with Kraichnan's[18] result for the ${}^{22}M$ mode mean square pressure in homogeneous, anisotropic turbulence with constant mean shear $\partial U_1/\partial x_2$.

Equation (22) allows us to write the low wavenumber spectral similarity law from Eq. (21) in the more useful form

$${}^{22}\Pi/\rho^2u^2S^2\ell^3={}^{22}G(k\ell) \tag{24}$$

where ${}^{22}G$ is a new function defined by absorbing ${}^{22}B^2$ into ${}^{22}G_p$.

At large Reynold's numbers, the high wavenumber components of the velocity spectrum are in a state of statistical equilibrium that is independent of large-scale structure of the flow, except for the dissipation rate ϵ which is determined by the rate at which the low wavenumber motions transfer energy to higher wavenumber motions. Since the pressure spectrum is determined by the velocity spectrum, it, too, should possess a similar equilibrium range of high wavenumbers, and the appropriate scales of length and velocity in this range must be the Kolmogorov scales,

$$\eta=(\nu^3/\epsilon)^{1/4} \tag{25}$$

and

$$v=(\epsilon\nu)^{1/4} \tag{26}$$

Then, following reasoning that is the same as that leading to Eqs. (22) and (23), the scale of the pressure variance for this equilibrium range must be $\rho^2\nu^2S^2\eta^2$. We note that even though S is a characteristic of the large-scale field, it must nonetheless appear in the small-scale pressure because, by definition, the ${}^{22}M$ mode fluctuations involve interactions with the mean shear. Physically, this pressure scale corresponds to pressure fluctuations created by small-scale velocity fluctuations, of order ν, interacting with the mean shear over distances of order η.

The appropriate nondimensional spectrum for high wavenumbers is ${}^{22}\Pi/\rho^2\nu^2S^2\eta^3$, and this must be a function of the dimensionless wavenumber $k\eta$, i.e.,

$${}^{22}\Pi/\rho^2\nu^2S^2\eta^3={}^{22}g(k\eta) \tag{27}$$

Here, unlike the low wavenumber spectrum, ${}^{22}G$, the function ${}^{22}g$ should be a universal function for all large Reynolds' number flows.

Equations (21) or (24) should be valid for $k\ll\eta^{-1}$, and Eq. (27) should be valid for $k\gg\ell^{-1}$. At very large Reynolds' numbers, such that $\ell^{-1}\ll\ll\eta^{-1}$, there should exist a subrange analogous to the inertial subrange of the velocity spectrum, in which $\ell^{-1}\ll k\ll\eta^{-1}$ and both Eq. (27) and Eqs. (21) or (24) are valid. The behavior of the pressure spectrum in this range can be determined by asympotically matching the large-scale and small-scale similarity laws in the limit of infinite Reynolds' number. Equating the pressure spectra from Eqs. (24) and (27) and rearranging them slightly gives $u^2\ell^3\,{}^{22}G=\nu^2\eta^3\,{}^{22}g$. Next, the well-known relation[5,6,16]

$$\epsilon\cong u^3/\ell \tag{28}$$

may be used to obtain the relation $\ell^{11/3}\,{}^{22}G=\eta^{11/3}\,{}^{22}g$. Since the ratio ℓ/η depends on the Reynolds' number,[6] both sides of the equation must be multiplied by $k^{11/3}$ in order to achieve matching, independent of the Reynolds' number. This gives

$$(k\ell)^{11/3}\,{}^{22}G(k\ell)=(k\eta)^{11/3}\,{}^{22}g(k\eta) \tag{29}$$

which cannot be valid unless both sides of the equation are equal to the same universal constant, ${}^{22}\alpha$. Thus, ${}^{22}G = {}^{22}\alpha(k\ell)^{-11/3}$, ${}^{22}g = {}^{22}\alpha(k\eta)^{-11/3}$ and the ${}^{22}M$ pressure spectrum obeys a $k^{-11/3}$ law in the inertial subrange through the relations

$$ {}^{22}\Pi/\rho^2 u^2 S^2 \ell^3 = {}^{22}\alpha(k\ell)^{-11/3} \tag{30a} $$

and

$$ {}^{22}\Pi/\rho^2 \nu^2 S^2 \eta^3 = {}^{22}\alpha(k\eta)^{-11/3} \tag{30b} $$

The constant ${}^{22}\alpha$ is the analog of Kolmogorov's constant for the velocity spectrum.

The analysis of the ${}^{04}\Pi$ and ${}^{13}\Pi$ spectra proceed in exactly the same manner as the preceding analysis of ${}^{22}\Pi$. The difference between these spectra arise from the essentially different manner in which pressure scales are related to the velocity and length scales, reflecting the different modes of interaction in each case.

In the case of the ${}^{04}M$ modes, an analysis similar to that for Eq. (22) yields

$$ {}^{04}\sigma_p^2 = {}^{04}B^2 \rho^2 u^4 \tag{31} $$

for the low wave number scale of pressure variance. This equation has been derived for isotropic turbulence by Batchelor,[5,19] Uberoi,[20] and Hinze[17] and for anisotropic turbulence by Kraichnan.[17] Batchelor estimated ${}^{04}B^2 \simeq 0.34$, while Uberoi[20] and Hinze[17] found somewhat higher values, ${}^{04}B^2 \simeq 0.5$. Kraichnan[18] related ${}^{04}B^2$ to anisotropy in homogeneous shear flow. The corresponding high wave number scale of pressure variance is $\rho^2 \nu^4$.

For the ${}^{13}M$ mode, the low and high wave number pressure scales are

$$ {}^{13}\sigma_p^2 = {}^{13}B^2 \rho^2 u^2 S\ell \tag{32} $$

and $\rho^2 \nu^3 S\eta$, respectively.

With these scales in hand, the arguments given for ${}^{22}\Pi$ can be repeated to give large and small wavenumber spectral similarity relations that are identical in form to Eqs. (27) and (24). Likewise, asymptotic matching arguments predict power law dependencies in the inertial subrange, a $k^{-7/3}$ power law for ${}^{04}\Pi$, and a k^{-3} power law for ${}^{13}\Pi$. These results are summarized in Table 1 and are consistent with Beuther et al.[10,11]

The total low wavenumber spectrum is given by the sum

$$ \Pi(k\ell) = \rho^2 u^4 \ell\, {}^{04}G(k\ell) + \rho^2 u^3 S\ell^2\, {}^{13}G(k\ell) + \rho^2 u^2 S^2 \ell^3\, {}^{22}G(k\ell), \quad k \ll \eta^{-1} \tag{33} $$

and, since each of these terms has a different pressure scale, it is not immediately apparent that total low wavenumber spectra can be correlated on a single plot. However, under the stated assumptions, the usual mixing length estimate, $u \sim S\ell$ is valid, and it folows that $u^3 S\ell \sim u^2 S^2 \ell^2 \sim u^4$. Then each modal component of the total spectrum possesses a pressure scale $\rho^2 u^4$ and the low wavenumber spectrum should exhibit similarity in the form

$$ \frac{\Pi}{\rho^2 u^4 \ell} = G(k\ell), \quad k \ll \eta^{-1} \tag{34} $$

All of the results stated in the preceding apply equally well the the one-dimensional spectrum with the substitutions $\Pi \to F_{pp}$, ${}^{22}\Pi \to {}^{22}F_{pp}$, ${}^{22}G \to {}^{22}H$, ${}^{22}g \to {}^{22}h$, and ${}^{22}\alpha \to (3/14)\,{}^{22}\alpha$, and so on for the other modes. This last factor of (3/14) follows by assuming that the inertial subranges of each mode are isotropic, so that Eq. (16) is applicable. The corresponding relations for the other two modes are ${}^{13}\alpha \to (1/6)\,{}^{13}\alpha$ and ${}^{04}\alpha \to (3/22)\,{}^{04}\alpha$.

III. Experiment

Jet Facility

The flow facility in which both velocity and pressure data were measured was an isothermal air flow simple jet with an exit diameter of 6.35 cm and exit velocity of 91.4 m/s. The nozzle contour, based on potential flow, gave a thin laminar boundary layer (0.0457 cm) at the jet exit with a flat mean velocity profile and a turbulence intensity which was sufficiently low ($\leq 0.2\%$) to cause no significant acoustical contamination. Further details of the flow system are given by Planchon.[4]

Figure 1 shows the flowfield geometry downstream of the nozzle exit. The three orthogonal coordinates $x_1 = x$, $x_2 = y$, and $x_3 = z$ show the axes used to define the flowfield and to locate the sensors. The velocity components corresponding to these axes are $u_1 = u$, $u_2 = v$, and $u_3 = w$, respectively.

Instrumentation

Velocity and fluctuating pressure data were obtained separately in this study. Two standard X-configuration hot-wire probes with 4-μ-diam tungsten sensors were used with DISA 55D01 model anemometers for the velocity measurements. These allowed two velocity components, either u and v or u and w, to be measured simultaneously at two points. Both convective and spatial scales, time and length, respectively, could be obtained for each velocity component. The velocity hot-wire sensors were operated with an overheat ratio of 1.8 and passed through BAY LAB 5123 low-noise amplifiers with a cutoff at -18dB/octave above 30 kHz. Prior to recording the four velocity signals on a SANGAMO FM tape recorder, TSI 1015C analog sum and difference correlators were used which provided ac coupling. The tape recorder was operated at 60 ips giving a frequency bandwidth of 20 kHz, which was well below the anemometer range and well above the energy containing frequency components in the flow. Planchon[4] has discussed in detail this instrumentation.

The fluctuating pressure was measured with a bleed-type pressure transducer. The transducer design and operating characteristics have been reported (for the original configuration) by Spencer and Jones[12] and for the modified configuration by Planchon.[4] Essentially, the probe uses a capillary bleed tube operated in laminar flow with a hot-film anemometer sensor mounted across its exit to measure the rate of bleed flow. The sensor and bleed tube are housed in a

Table 1 Spectral similarity laws for the ${}^{04}M$, ${}^{13}M$, and ${}^{22}M$ interaction modes

Spectral mode	$k \ll\ll \eta^{-1}$	$\ell^{-1} \ll k \ll \eta^{-1}$			$k \gg\gg \ell^{-1}$
${}^{04}\Pi$	$\rho^2 u^4 \ell\, {}^{04}G(k\ell)$	${}^{04}\alpha\rho^2 u^4 \ell (k\ell)^{-7/3}$	or	${}^{04}\alpha\rho^2 \nu^4 \eta (k\eta)^{-7/3}$	$\rho^2 \nu^4 \eta\, {}^{04}g(k\eta)$
${}^{13}\Pi$	$\rho^2 u^3 S\ell^2\, {}^{13}G(k\ell)$	${}^{13}\alpha\rho^2 u^3 S\ell^2 (k\ell)^{-3}$	or	${}^{13}\alpha\rho^2 \nu^3 S\eta^2 (k\eta)^{-3}$	$\rho^2 \nu^3 S\eta^2\, {}^{13}g(k\eta)$
${}^{22}\Pi$	$\rho^2 u^2 S^2 \ell^3\, {}^{22}G(k\ell)$	${}^{22}\alpha\rho^2 u^2 S^2 \ell^3 (k\ell)^{-11/3}$	or	${}^{22}\alpha\rho^2 \nu^2 S^2 \eta^3 (k\eta)^{-11/3}$	$\rho^2 \nu^2 S^2 \eta^3\, {}^{22}g(k\eta)$

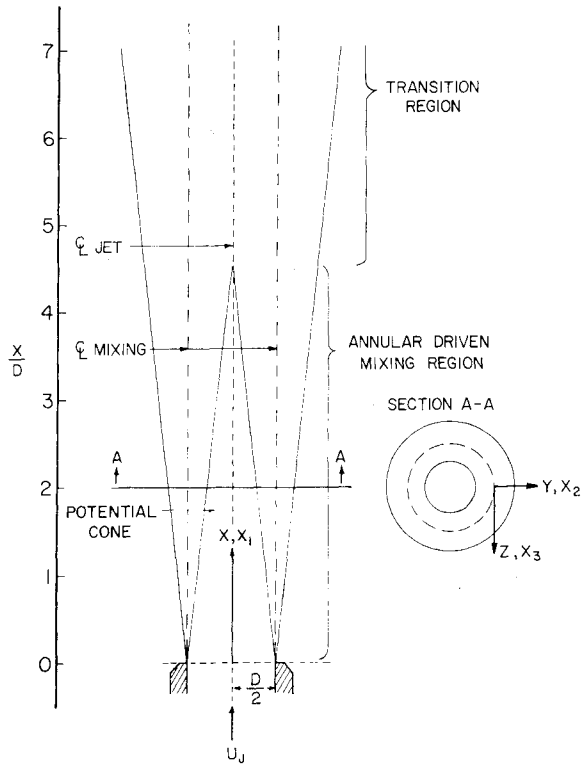

Fig. 1 Jet nozzle and flow coordinate system.

1.52-mm-diam tube which has a hemispherical tip on the upstream end and six bleed holes 3.75-mm downstream from the tip and located evenly about the probe circumference. A constant-pressure air supply provides a bleed flow which is modulated by changes in the ambient pressure surrounding the probe. The bleed flow velocity is linearly dependent on the differential pressure across the bleed tube.

Using an overheat ratio of 1.6 and mean differential pressure of 15 cm of water, the signal-to-noise ratio at the mixing layer centerline was greater than 20 to 1, and frequency response was flat to 10 kHz. Estimates of the contamination from tranverse velocity fluctuations using yaw tests showed maximum error values of 5% in pressure intensity for shear layers with mean velocities greater than 15 m/s. Two matched probes were used simultaneously to obtain both convected field and spatial structure of the turbulent pressure fluctuations.

Procedures

The region of primary examination in this study is the centerline of the driven mixing layer ($y=0$ in Fig. 1) of the jet from the jet exit to six diameters downstream. In this region flow reversals are unlikely and large yaw angles by the flow are infrequent. Because both mean shear and turbulent intensity are large, it provides large pressure fluctuations which can be accurately measured.

The velocity sensors or pressure sensors were mounted on traversing supports which provided full three-dimensional positioning with separation. Mean values of jet velocity were obtained from anemometer data as well as from isentropic nozzle flow relations.

Convective and spatial structure were obtained with a 100-point SAICOR Correlation Analyzer. One-dimensional energy spectra were evaluated with a General Radio Spectral Analyzer using a 1/10th octave bandpass. rms values were measured directly with a TSI true rms meter and the average rms velocity u was evaluated from $u=[\frac{1}{3}(\overline{u^2}+\overline{v^2}+\overline{w^2})]^{\frac{1}{2}}$. The convection velocity U_c and the integral scales, of length, L_u^x and L_u^y, and time were evaluated from the space-time covariance for each quantity, i.e., for pressure the covariance is $C_{pp}(r,\tau)=\overline{p(x,t)p(x+r,t+\tau)}$. By fitting an envelope to covariances with different axial separation, the convection integral time scale and convection velocity U_c were obtained. For zero time delay, the true, two-point spatial covariances were formed, from which the integral length scales L_u^x and L_v^x were found.

Normalized spectra in wavenumber space were formed from the measured frequency spectra by employing Taylor's hypothesis. The one-dimensional frequency spectrum, $F_n(f)$, was defined such that

$$\int_0^\infty F_n(f)\,df=1$$

and the wavenumber was defined by $k_1=2\pi f/U_c$. The resulting wavenumber spectrum, e.g., for the streamwise velocity component $u=u_1$, was obtained from

$$F_{11}(k_1)=\frac{U_c\sigma_u^2}{4\pi}F_n(f)\Big|_{f=(k_1U_c/2\pi)}$$

where the experimentally determined value of U_c was nearly equal to the mean velocity along the centerline of the driven mixing layer and varied slightly about the nominal value of $0.66\ U_j$. The procedures used to evaluate the turbulent dissipation rate, ϵ, will be discussed in conjunction with the velocity spectra presented in the next section.

IV. Results and Discussion

Large-Scale Flow Properties

The rms velocities, rms pressure, and integral length scales have been examined in order to specify the large-scale properties of the flow and to assess the extent to which the driven mixing layer exhibited self-preservation. rms values along the centerline of the mixing layer are presented in Table 2, wherein U_j and ρU_j^2 have been used as the scales of velocity and pressure so that the physical rms values can be recovered from the dimensionless results. The flow was significantly anisotropic along the centerline, the average ratio of $\sigma_u:\sigma_v:\sigma_w$ being 1:0.75:0.71 with an average turbulence intensity of about 12.5% between $x/D=2$ and $x/D=6$. The rms velocities were relatively constant in this range, indicating a very nearly self-preserving flow, although there was a slight tendency towards increasing turbulence intensity between the jet exit and $x/D=4$. This is attributed to a weak development of the mixing layer associated with the finite width of the lip of the jet nozzle. Likewise, the rms pressure is also nearly constant along the centerline, although Planchon[4] has reported data out to $x/D=10$ which show decreasing pressure intensity beyond the end of the potential cone at $x/D=5$, where the flow begins to make a transition between a pure mixing layer and a fully developed free jet. Thus, the most nearly self-preserving region of the centerline flow was in the range $x/D=3$ to $x/D=5$.

The average of the values of $\sigma_p/\rho u^2$ listed in Table 2 yields $\sigma_p\cong 2\rho u^2$. This result provides some indication of the relative contributions that the various interaction modes make to the

Table 2 Flow properties on the mixing layer centerline, $y=0$[a]

$\frac{X}{D}$	$\frac{\sigma_u}{U_J}$	$\frac{\sigma_v}{U_J}$	$\frac{\sigma_w}{U_J}$	$\frac{u}{U_J}$	$\frac{\sigma_p}{\rho U_J^2}$	$\frac{\sigma_p}{\rho u^2}$
2	0.140	0.114	0.100	0.119	0.030	2.12
3	0.145	0.108	0.105	0.121	0.032	2.18
4	0.151	0.113	0.109	0.126	0.032	2.02
5	0.153	0.112	0.108	0.126	0.030	1.89
6	0.156	0.112	0.107	0.127	0.029	1.80

[a] $U_J=91.4\ \text{ms}^{-1}$, $D=6.35$ cm.

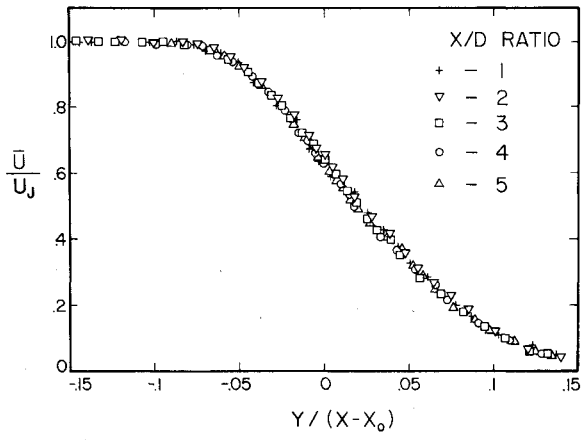

Fig. 2 Mean velocity in the driven mixing layer: $x_0 = -1.02$ cm, $D = 6.35$ cm, $U_J = 91.4$ m/s.

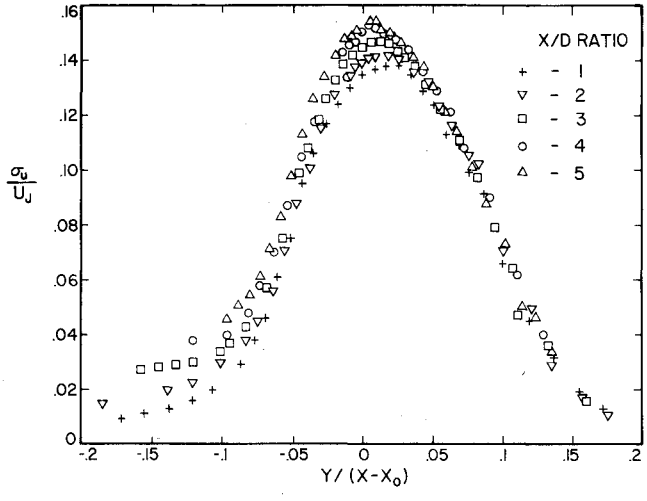

Fig. 3 rms streamwise velocity profiles in the driven mixing layer: $x_0 = -1.02$ cm, $D = 6.35$ cm, $U_J = 91.4$ m/s.

total mean square pressure in this flow. Since the magnitudes of the measured skewness functions for the various velocity components were small (less than 0.1), we shall assume that the ^{13}M mode contribution was negligible. Then, according to Eq. (11) $\sigma_p^2 \cong {}^{22}\sigma_p^2 + {}^{04}\sigma_p^2$, and the ${}^{04}\sigma_p^2$ contribution can be estimated by using the results for isotropic turbulence,[17] ${}^{04}\sigma_p^2 \cong 0.5\,\rho^2 u^4$. This yields ${}^{22}\sigma_p^2 \cong 3.5\,\rho^2 u^4$. Hence, the ^{22}M (turbulent-mean shear) mode contributes almost seven times as much to the mean square pressure as the ^{04}M (turbulent-turbulent) mode. This result is not unexpected in view of the high shear rate in the mixing layer flow, and it is consistent with the estimates made by Planchon.[4]

Self-preservation of the shear layer profiles is demonstrated for the mean velocity in Fig. 2, for the rms value of the streamwise velocity in Fig. 3, and the rms pressure in Fig. 4. The corresponding profiles of σ_v and σ_w were similar to Fig. 3. A virtual origin $x_0 = -1.02$ cm was needed in each of the profiles to collapse the data, indicating that the mixing layer had already achieved a finite thickness at $x = 0$ because of the width of the nozzle lip. Mixing layer development is particularly evident between $x/D = 1$ and $x/D = 3$ for the pressure intensity profiles shown in Fig. 4. As before, the most nearly self-preserving region lies around three to five jet diameters downstream of the exit.

Velocity Spectrum Similarity

Since the pressure spectrum is ultimately determined by the velocity field we have examined the velocity spectra in detail, particularly in regard to their similarity in the various spectral

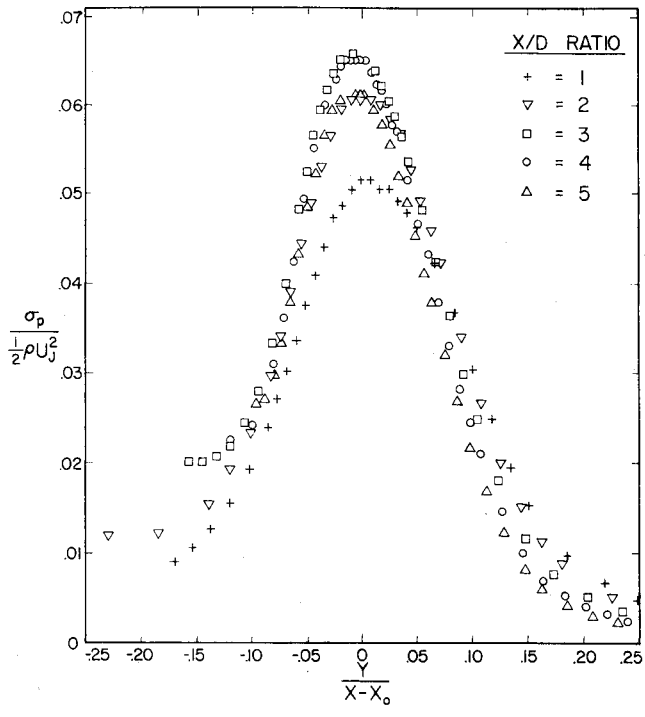

Fig. 4 rms pressure profiles in the driven mixing layer: $x_0 = -1.02$ cm, $D = 6.35$ cm, $U_J = 91.4$ m/s.

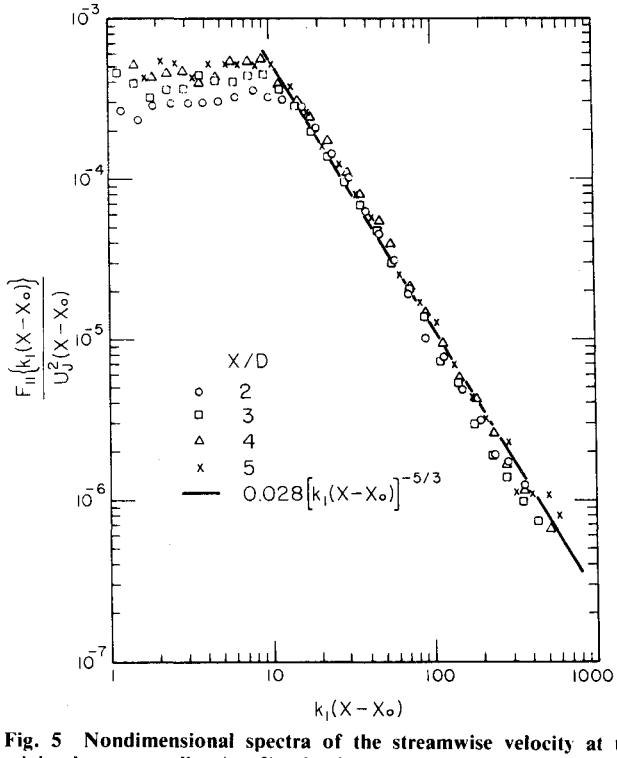

Fig. 5 Nondimensional spectra of the streamwise velocity at the mixing layer centerline ($y = 0$) using large-scale parameters: $U_J = 91.4$ m/s, $x_0 = -1.02$ cm, $D = 6.25$ cm.

ranges. Low wave number similarity plots of the one-dimensional u and v spectra are presented in Figs. 5 and 6 wherein the parameters U_J and $(x - x_0)$ have been used for the low wave number scaling in place of u and ℓ in order to avoid any uncertainties in the experimental evaluation of u and ℓ. This choice of scales is justified by the relatively constant values of u/U_J and $L_u^x/(x - x_0)$ shown in Tables 2 and 3. The data collapse very well in the inertial subrange where $k_1^{-5/3}$ power law behavior is evident over almost two decades of

Table 3 Kolmogorov scales and related quantities on the mixing layer centerline

x/D	$\frac{L_u^{x\,a}}{x-x_0}$	$\frac{u^3/\frac{1}{2}L_u^x}{U_J^3/D}$	ν, ms^{-1}	η, m$\times 10^5$
2	...	0.0102	1.167	1.286
3	0.153	0.0083	1.106	1.356
4	0.149	0.0073	1.061	1.414
5	0.153	0.0060	1.021	1.469
6	0.153	0.0049	0.938	1.550

[a] $x_0 = -1.02$ cm.

wavenumber. The solid lines are our best $k_1^{-5/3}$ law fits. At lower wavenumbers the F_{22} spectra also collapse very well, but the F_{11} spectra show somewhat greater scatter. Part of this scatter is due to the lack of self-preservation at $x/D=2$, suggesting that the data at this location should be ignored in tests for low wave number spectral similarity.

Similarity plots of the u and v spectra using Kolmogorov scaling are shown in Figs. 7 and 8. As expected, this nondimensionalization no longer correlates the low wave number ends of the spectra, but continues to show similarity in the inertial subrange and beyond.

We note that isotropy of the small-scale motions in the inertial subrange would require that $F_{22}=4/3F_{11}$. In contrast, our best fits show $F_{22}\simeq F_{11}$ in this range in Figs. 7 and 8, and $F_{22}\simeq 0.75\ F_{11}$ from the power law fits in Figs. 5 and 6. We attribute these differences to errors in the experimentally measured ratio σ_u/σ_v due to large turbulence intensity and in the determination of the power law fits, rather than evidence of small-scale anisotropy. For instance, a 20% decrease in σ_u/σ_v would increase F_{22}/F_{11} by 44%, and selecting power law fits at higher wavenumber in Figs. 5 and 7 would have increased F_{22}/F_{11} by about 25%.

The value of ϵ needed to calculate ν and η could not be determined by direct evaluation of the mean square time derivative because of frequency response limitations in these experiments. We estimated ϵ indirectly by using Eq. (28) with ℓ set equal to the measured values of $\frac{1}{2}L_u^x$. This gave the dimensionless dissipation rates shown in the second column of Table 3, from which the estimated values of ν and η were calculated. The accuracies of these estimates were confirmed by the fact that they produced normalized u spectra in Fig. 7 whose inertial subrange power laws agreed with the accepted value of 0.25 $(k_1\eta)^{-5/3}$. (Townsend[15] quotes 0.50 ± 0.03 for one-sided spectra, corresponding to 0.25 ± 0.015 for our two-sided spectra.)

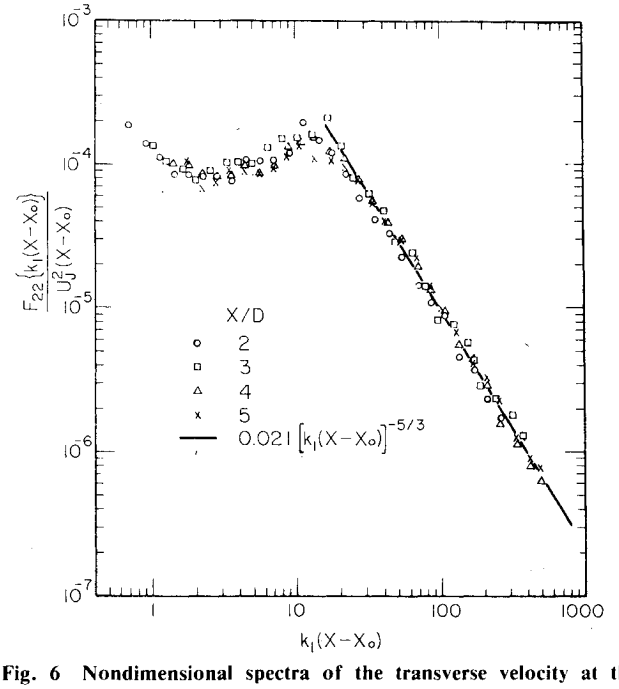

Fig. 6 Nondimensional spectra of the transverse velocity at the mixing layer centerline ($y=0$) using large-scale parameters: $U_J=91.4$ m/s, $x_0=-1.02$ cm, $D=6.35$ cm.

Pressure Spectrum Similarity

The pressure spectra at several downstream locations on the centerline of the driven mixing layer are presented in Figs. 9-

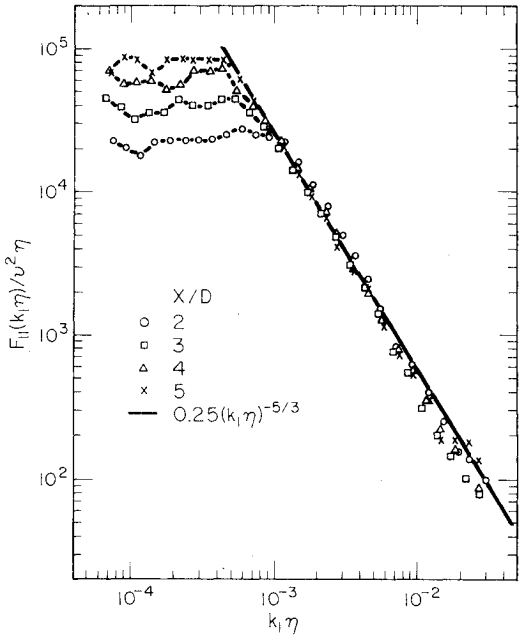

Fig. 7 Nondimensional spectra of the streamwise velocity at the mixing layer centerline ($y=0$) using the Kolmogorov scales ν and η: $U_J=91.4$ m/s, $x_0=-1.02$ cm, $D=6.35$ cm.

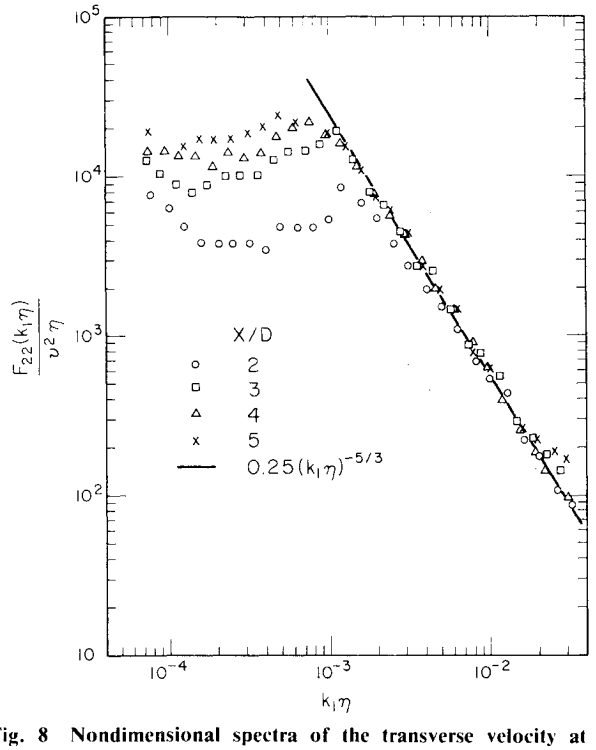

Fig. 8 Nondimensional spectra of the transverse velocity at the mixing layer centerline ($y=0$) using the Kolmogorov scales ν and η: $U_J=91.4$ m/s, $x_0=-1.02$ cm, $D=6.35$ cm.

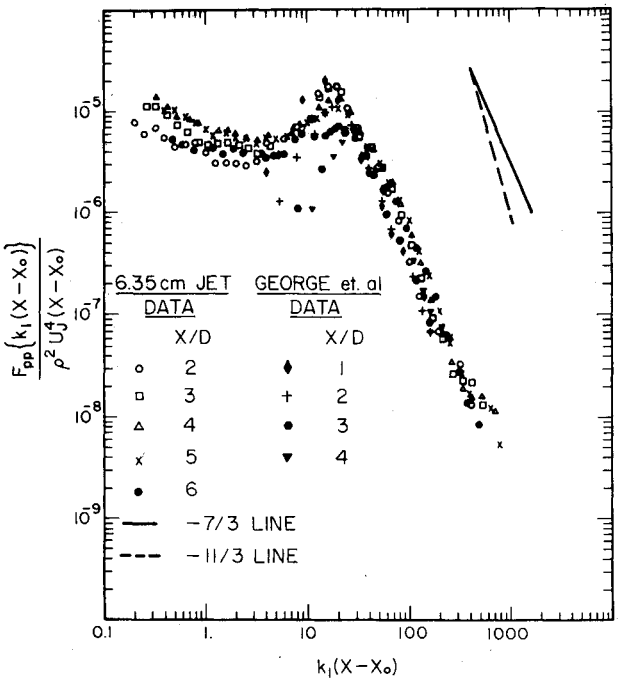

Fig. 9 Nondimensional spectra of the fluctuating pressure at the mixing centerline ($y=0$) using large-scale parameters: $U_J=-91.4$ m/s, $x_0=-6.35$ cm, $D=6.35$ cm. The data of Beuther et al.[10,11] are shown for comparison.

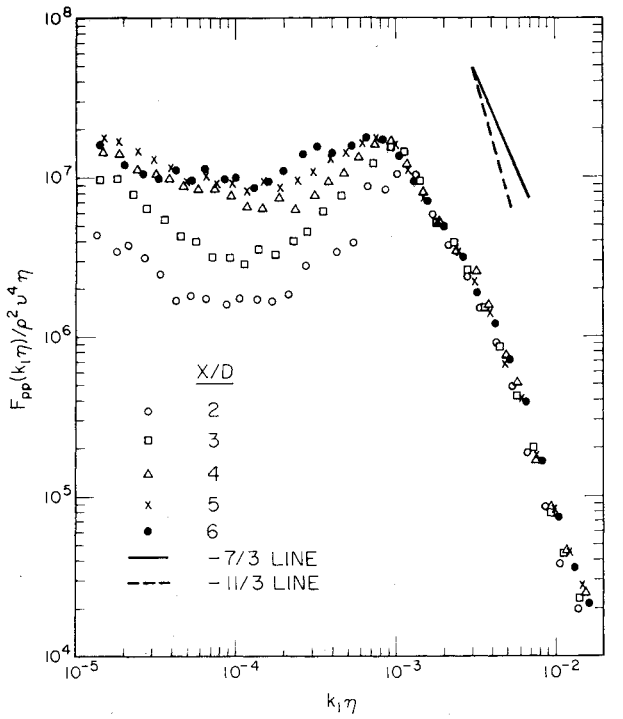

Fig. 10 Nondimensional spectra of the fluctuating pressure at the mixing centerline ($y=0$) using the Kolmogorov scales ν and η in the form appropriate for the ^{04}M mode: $U_J=91.4$ m/s, $x_0=-6.35$ cm, $D=6.35$ cm.

11. When interpreting these data it is important to recall from Eq. (18) that the total spectrum F_{pp} is the sum of the three modal spectra, $^{04}F_{pp}+{}^{13}F_{pp}+{}^{22}F_{pp}$. Low wave number similarity is examined in Fig. 9 where the velocity and length scales of the large-scale motions, u and ℓ, respectively, have been replaced by U_J and $x-x_0$ as in the velocity spectra shown in Figs. 5 and 6. According to the arguments leading to Eq. (34), the low wavenumber ends of each of the one-

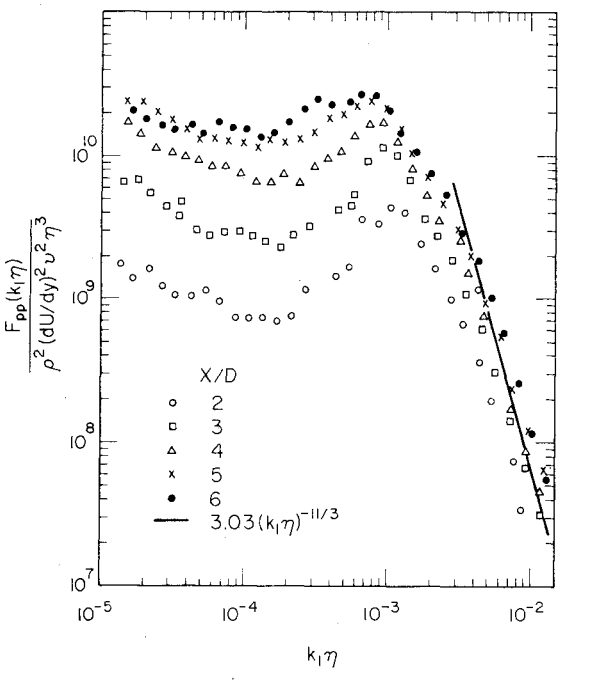

Fig. 11 Nondimensional spectra of the fluctuating pressure at the mixing centerline ($y=0$) using the Kolmogorov scales ν and η and the shear gradient dU/dy in the form appropriate for the ^{22}M mode: $U_J=91.4$ m/s, $x_0=-6.35$ cm, $D=6.35$ cm.

dimensional spectral modes $^{04}F_{pp}$, $^{13}F_{pp}$, and $^{22}F_{pp}$ should exhibit similarity under such scaling (assuming self-preservation) so, the total spectrum $F_{pp}=^{04}F_{pp}+{}^{13}F_{pp}+{}^{22}F_{pp}$ should also exhibit similarity. Essentially, $F_{pp}(k_1(x-x_0))/\rho^2U_J^4(x-x_0)$ is the one-dimensional spectral analog of the quantity $G(k_1\ell)$ appearing in Eq. (34). In the inertial subrange lying to the right of the spectral peak located at about $k_1(x-x_0)=20$ similarity is found at all downstream locations for our data. To the left of the spectral peak, e.g., at the low wavenumbers where self-preservation is required for similarity, our data at $x/D=3,4,5$ are closely similar, while the data for the non-self-preserving locations, $x/D=2$ and $x/D=6$, are less so. This is as expected. However, in comparison with the velocity structure, the virtual origin for the pressure spectra is -6.35 cm rather than -1.02 cm. This suggests a different rate of pressure structure development, but the details of this discrepancy are not fully understood at this time.

For purposes of comparison, the data by Beuther et al.[10,11] are also presented in Fig. 9. The value of the virtual origin was $x_0=0$ for these data because the experiments were performed in a much larger jet with a smaller lip. The general consistency between their data and ours; taken with different instruments in flows with considerably different scales lends credence to the veracity of both the measurements and the similarity theory. There are, however, nonnegligible differences between the two experiments, particularly in the low wavenumber region below the spectral peak where the data of Beuther et al.[10,11] fail to collapse and show a surprisingly sharp peak in the spectra. Also, rather broad scatter in the inertial subrange obscures a well-defined shape that is evident when our data are plotted alone.

Two different similarity plots of the pressure spectra using Kolmogorov scaling are presented in Figs. 10 and 11. The pressure scaling used in Fig. 10 is appropriate for similarity of the ^{04}M mode spectra while the scaling used in Fig. 11 is appropriate for similarity of the ^{22}M mode spectra. Since F_{pp} is the sum of these modes plus the ^{13}M mode, neither type of plot guarantees similarity of the total spectrum, but, in fact, the ^{04}M mode scaling in Fig. 10 does display strong similarity

in the inertial subrange, perceptably more so than the ^{22}M mode scaling in Fig. 11.

The combined effects of the ^{04}M, ^{13}M, and ^{22}M spectra should produce a slope in the inertial subrange that lies somewhere between the slope of a $k_1^{-7/3}$ and $k_1^{-11/3}$ power law. The slope of the data does lie between these limits over a significant range of wave numbers and is somewhat closer to the $k_1^{-11/3}$ law. At larger wavenumbers we expect the ^{04}M mode to become dominant because the ^{22}M mode contribution is decreasing more rapidly than the ^{04}M mode contribution. However, the data do not extend to wavenumbers large enough to demonstrate such behavior.

Since the effects of the three modes are confounded in Figs. 10 and 11 we cannot properly evaluate the universal constants $^{04}\alpha$, $^{13}\alpha$, and $^{22}\alpha$. In particular, the value of 3.03 in the best $k_1^{-11/3}$ fit shown in Fig. 11 should only be interpreted as an upper bound for the value of $^{22}\alpha$. The values of $^{04}\alpha$, $^{13}\alpha$, and $^{22}\alpha$ could conceivably be estimated by postulating a more detailed spectral model or by fitting a combination of the $k_1^{-7/3}$, $k_1^{-9/3}$, and $k_1^{-11/3}$ power laws to the data, but we have not attempted such an evaluation here.

V. Conclusions

This study has, through dimensional arguments, predicted the spectral similarity laws associated with pressure spectra in self-preserving turbulent flows. Experimental data for a turbulent shear layer have been obtained and compared with these laws. The experimental results generally support the similarity theory, although direct verification of the various inertial subrange power laws and their associated constants was not obtained. Evidence was cited which suggests a tendency for the ^{22}M mode to dominate the large-scale structure of the driven mixing layer.

The mutual agreement between our data, the data of Beuther et al.[10,11] and the similarity theory strongly supports the veracity of the unsteady pressure transducers used in both experiments. This suggests that significant experimental studies of previously inaccessible pressure fluctuations can be pursued successfully. The marked difference between the inertial subrange of the velocity spectra, which clearly obeyed a $k_1^{-5/3}$ power law and the pressure spectra, which showed little, if any, $k_1^{-5/3}$ behavior, further indicates that there was little velocity contamination in the pressure transducer signal.

Acknowledgments

The authors express their appreciation for the support for the experimental portion of this study by NASA-Lewis Research Center under grant NASA NGR 14-005-149, and the assistance of T. Hammerich in evaluating some of the spectra.

References

[1] Daly, B. J. and Harlow, F. H., "Transport Equations in Turbulence," *Physics of Fluids*, Vol. 13, Nov. 1970, pp. 2634-2649.

[2] Lumley, J. L. and Khajeh-Nouri, B., "Computational Modeling of Turbulent Transport," *Advances in Geophysics*, Vol. 18A, 1974, pp. 169-192.

[3] Ribner, H. S., "The Generation of Sound in Turbulent Jets," *Advances in Applied Mechanics*, Vol. 8, edited by H. L. Dryden, T. Von Karman, and G. Kuerti, Academic Press, New York, 1964, pp. 103-187.

[4] Planchon, H. P., Jr., "The Fluctuating Static Pressure Field in a Round Jet Turbulent Mixing Layer," Ph.D. Thesis, University of Illinois at Urbana-Champaign, 1974.

[5] Batchelor, G. K., *The Theory of Homogeneous Turbulence*, Cambridge University Press, Cambridge, 1953.

[6] Tennekes, H. and Lumley, J. L., *A First Course in Turbulence*, MIT Press, Cambridge, Mass., 1972.

[7] George, W. K., "The Equilibrium Range of Turbulent Pressure Spectra," *Bulletin of the American Physical Society*, Vol. 19, Nov. 1974, p. 1158 (abstract).

[8] Fuchs, H. V., "Measurement of Pressure Fluctuations with Microphones in an Airstream," Institute of Sound and Vibration Research, University of Southampton, Memo. 281, Nov. 1969.

[9] Hammersley, R. J., "An Experimental Investigation of the Turbulent Characteristics of Co-Annular Jets and Their Role in Aerodynamic Noise Generation," Ph.D. Thesis, University of Illinois at Urbana-Champaign, 1974.

[10] Beuther, P. D., Georege, W. K., and Arndt, R.E.A., "Modeling of Pressure Spectra in a Turbulent Shear Flow," *Acoustical Society of America Meeting*, State College, Pa., June 6-10, 1977.

[11] Beuther, P. D., George, W. K., and Arndt, R.E.A., "Pressure Spectra in a Turbulent Shear Flow," *Bulletin of the American Physical Society*, Vol. 22, 1977, p. 1285 (abstract).

[12] Spencer, B. W. and Jones, B. G., "A Bleed-type Pressure Transducer for In-Stream Measurement of Static Pressure Fluctuations," *Review of Scientific Instruments*, Vol. 42, April 1971, pp. 450-454.

[13] Arndt, R.E.A. and Nilsen, A. W., "On the Measurement of Fluctuating Pressure in the Mixing Zone of a Round Jet," ASME No. 71-FE-31, 1971.

[14] Adrian, R. J., Jones, B. G., Chung, M. K., and Nithianandan, C. K., "Linear Estimation Closures of Two-Point Conditional Averages in Turbulent Jets," *Bulletin of the American Physical Society*, Vol. 21, Nov. 1976, p. 1233 (abstract).

[15] George, W. K. and Beuther, P. D., "Pressure Spectra in Homogeneous, Istotropic Turbulent Flow," *Bulletin of the American Physical Society*, Vol. 22, Nov. 1977, p. 1285 (abstract).

[16] Townsend, A. A., *The Structures of Turbulent Shear Flow*, Cambridge University Press, Cambridge, 1975.

[17] Hinze, J. O., *Turbulence*, McGraw-Hill, New York, 1975.

[18] Kraichnan, R. H., "Pressure Field within Homogeneous, Anisotropic Turbulence," *Journal of the Acoustical Society of America*, Vol. 28, Jan. 1956, pp. 64-72.

[19] Batchelor, G. K., "Pressure Fluctuations in Isotropic Turbulence," *Proceedings of the Cambridge Philosophical Society*, Vol. 47, April 1951, p. 359.

[20] Uberoi, M. S., "Correlations Involving Pressure Fluctuations," NASA TN 3116, 1954.